nature geoscience

ARTICLES

PUBLISHED ONLINE: 24 NOVEMBER 2014 | DOI: 10.1038/NGEO2299

Thick and deformed Antarctic sea ice mapped with autonomous underwater vehicles

G. Williams[1,2*†], T. Maksym[3*†], J. Wilkinson[4*†], C. Kunz[3,5], C. Murphy[6], P. Kimball[3] and H. Singh[3]

Satellites have documented trends in Antarctic sea-ice extent and its variability for decades, but estimating sea-ice thickness in the Antarctic from remote sensing data remains challenging. *In situ* observations needed for validation of remote sensing data and sea-ice models are limited; most have been restricted to a few point measurements on selected ice floes, or to visual shipboard estimates. Here we present three-dimensional (3D) floe-scale maps of sea-ice draft for ten floes, compiled from two springtime expeditions by an autonomous underwater vehicle to the near-coastal regions of the Weddell, Bellingshausen, and Wilkes Land sectors of Antarctica. Mean drafts range from 1.4 to 5.5 m, with maxima up to 16 m. We also find that, on average, 76% of the ice volume is deformed ice. Our surveys indicate that the floes are much thicker and more deformed than reported by most drilling and ship-based measurements of Antarctic sea ice. We suggest that thick ice in the near-coastal and interior pack may be under-represented in existing *in situ* assessments of Antarctic sea ice and hence, on average, Antarctic sea ice may be thicker than previously thought.

Antarctic sea-ice extent has seen an overall positive trend with large regional variability over the past three decades[1], the causes of which remain under debate[2–5]. Some models suggest greater trends in ice thickness[6,7], providing another metric with which to evaluate sea-ice–climate interactions. However, there remains considerable uncertainty in even the climatological large-scale distribution of Antarctic sea-ice thickness, its smaller scale distribution (that is, the degree of deformation), and seasonal variability. This uncertainty limits our ability to evaluate sea ice and climate models[6,8] and the role of sea-ice deformation in controlling ice thickness[7], ice production[9], and ice–ocean buoyancy forcing[10].

While US and British submarines have been critical in the monitoring of Arctic sea-ice thickness[11], no similar data set exists for the Antarctic. Direct *in situ* measurements are restricted to short drilling profiles (~100–200 drill holes per floe)[12]. Draft measurements from upward looking sonar (ULS) are available during several years, but only for the Weddell Sea[13,14]. While a small number of electromagnetic measurements of sea-ice thickness have also been made, there are known limitations in areas of thick, deformed ice[15,16]. The only circumpolar estimate of sea-ice thickness is from visual estimates of thickness from ships while underway[17].

All these data suggest a relatively thin ice cover (mean ~ 1 m), although some limited observations of much thicker ice have been observed[13,14], mostly in late spring and summer[15,17–19]. Available data from 20 cruises[12,20,21] find only one drilling profile with a mean thickness of over 3 m (3.1 m), with very few individual drill holes greater than 5 m thick. It is known that drilling profiles tend to avoid the thickest ice[19]. Some model estimates of ice thickness distribution are comparable to *in situ* observations[22,23], whereas others tend to show slightly thicker ice[6,7].

A selection bias may exist in the observations due to ships avoiding areas of thicker ice[22]. By late winter, ships cannot penetrate into the heavy ice typically found in the interior pack and along the coast[20,24]. This thick ice is generally observed only in summer, when the open pack permits access[18]. Satellite-based estimates suggest extensive areas of thicker ice in the interior pack[25–27], but regional estimates vary significantly, largely due to uncertainty in snow cover[25,27,28]. At present, the extent and volume of thick, inaccessible ice in late winter and spring, and, hence, the mean thickness of the entire pack, is uncertain.

Recent advances in autonomous underwater vehicle (AUV) technology have opened up access to the sea-ice underside, allowing a 'new view' of the thickness distribution in the Arctic[29]. No comparable data set has been available for the Antarctic. Here we present ten floe-scale maps of sea-ice draft collected by AUV missions undertaken during two recent early spring voyages (IceBell and SIPEX-2, see Methods and Supplementary Information) in three regional sectors around Antarctica. With a combined areal coverage of over 500,000 m^2 (Table 1), this is the most comprehensive—and only—high-resolution 3D view of Antarctic sea-ice morphology to date. These maps reveal heavy deformation in all three near-coastal regions, producing a mean sea-ice draft well in excess of that typically observed from drilling data. Such thick ice is under-represented in current assessments of Antarctic sea-ice thickness distribution.

Floe-scale maps of early spring sea-ice draft

Sea-ice floes in each of the three regions were surveyed in mid to late spring. Owing to the proximity to the continent (Fig. 1), the ice may have developed over the entire season in some cases. Although some sea ice from the previous winter can survive the summer melt season in each of the sample regions and become re-incorporated in the following winter's pack, all the surveyed floes were determined to most likely be first-year ice (Supplementary Information).

Bellingshausen Sea continental shelf

The sea-ice draft maps demonstrate the highly deformed nature of the surveyed sea ice in the southern Bellingshausen Sea (Fig. 2a).

[1]Institute of Antarctic and Marine Science, University of Tasmania, Hobart, Tasmania 7004, Australia. [2]Antarctic Climate & Ecosystems Cooperative Research Centre, Hobart, Tasmania 7004, Australia. [3]Woods Hole Oceanographic Research Institution, Woods Hole, Massachusetts 02543, USA. [4]British Antarctic Survey, Cambridge CB2 1RT, UK. [5]Google Inc., Mountain View, California 94043, USA. [6]Bluefin Robotics, Quincy, Massachusetts 02169, USA. †These authors contributed equally to this work. *e-mail: guy.darvall.williams@gmail.com; tmaksym@whoi.edu; jeremy.wilkinson@bas.ac.uk

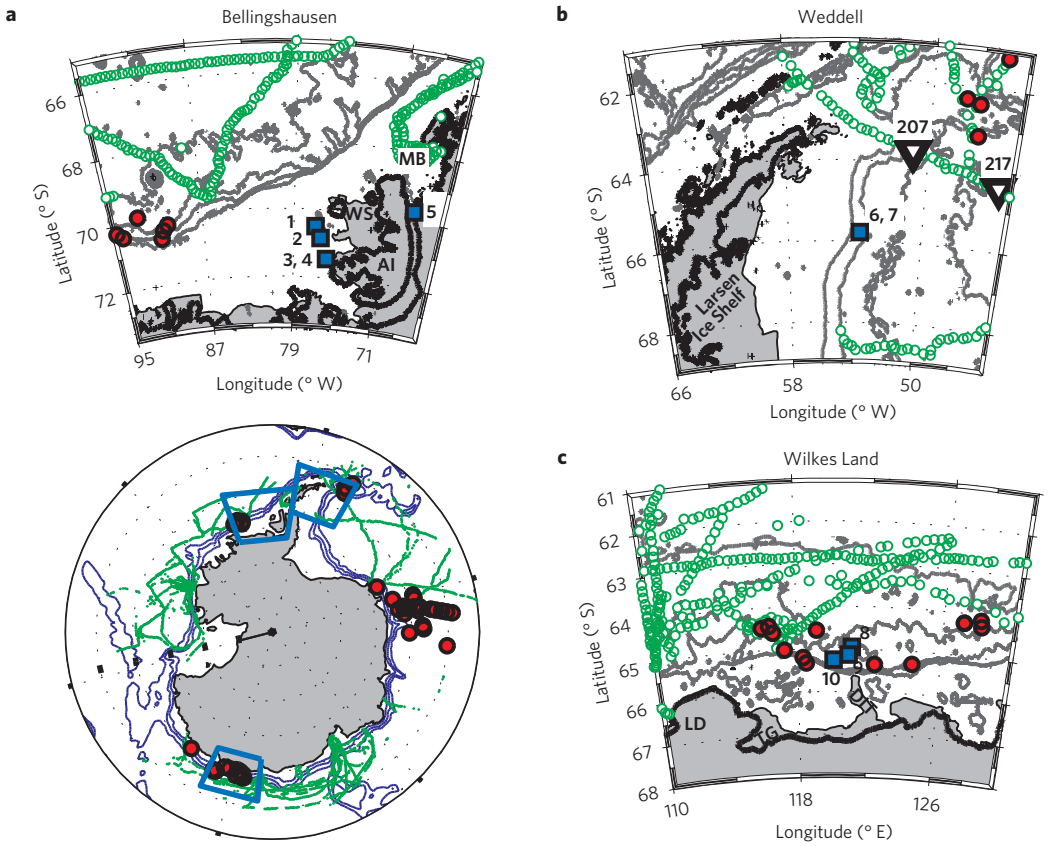

Figure 1 | IceBell and SIPEX-2 Study areas. a, IceBell Floes 1–5 in the Bellingshausen Sea (blue squares). **b**, IceBell Floes 6–7 in the north-west Weddell Sea. Location of nearby ULS data[14] is indicated by black triangles (sites 207 and 217). **c**, SIPEX-2 Floes 8–10 offshore from Wilkes Land, East Antarctica. Previous ASPeCt ship-based observations[17] for September through November (open green circles) and drill data[12] (larger red circles, Supplementary Table 2) used for comparison are also shown. Inset: Regional study areas for **a**–**c** (blue boxes) and circumpolar data (Fig. 3 and Table 1).

Floe 1 was a rubble field, composed of refrozen broken ice that forms an essentially 100% deformed ice floe, with a mean draft of 5.5 m and maximum of 11.5 m (Table 1). This is significantly thicker than any previously surveyed first-year floe from drilling data in the Antarctic[12]. The draft distribution forms a broad, flat, bell shape around this mean, with a small peak at ~1.8 m indicative of the 'level' ice draft (Supplementary Fig. 3a). The 3D map reveals no clearly defined, linear ridges. These characteristics suggest the floe formed from the congelation of broken floes and brash, possibly generated by repeated collisions of floes that had then been compressed together.

Other floes surveyed in the Bellingshausen Sea contained more level ice (Fig. 2a, Floes 2–3, modal drafts of 1.4 and 1.2 m, respectively) separated by quasi-linear features resembling pressure ridges. The maps show that these deformation features formed through refreezing of rubble around the edges of smaller, rounded ice pans. This rubble is clearly seen in Floe 2, which has a prominent second mode in the ice draft distribution at ~3.5 m, and a long, flat tail extending up to 10.8 m draft for Floe 4 (Supplementary Fig. 3). Despite a significant quantity of relatively level ice in Floes 4 and 5, the modal draft of these floes (2.0 and 2.7 m, respectively) is thicker than commonly can be achieved thermodynamically in first-year ice. Heavy snow accumulation may contribute, but the broad draft distribution (Supplementary Fig. 3) indicates thickening through extensive deformation.

North-west Weddell Sea continental slope

Two adjacent floes were surveyed in the north-west Weddell Sea in November 2010, at the boundary between first-year ice to the east and predominantly multiyear ice to the west. These floes (Fig. 2b, floe 6 and 7) have modal drafts of 1.2–1.5 m, indicating thick first-year ice. Floe 7 was composed predominantly of undeformed ice, indicated by the sharp peak at 1.2 m in the draft distribution (Fig. 3b and Supplementary Fig. 3). This peak is also in Floe 6 (Supplementary Fig. 3), but the large standard deviation of the draft (Table 1), a mean draft of 3.1 m (2.6 times the level ice draft) and a maximum draft exceeding 13 m (Table 1) indicate heavy deformation. The variance in ice draft on scales of ~100 m for these two floes demonstrates that larger floes, consisting of smaller floes with different structural histories, require large survey length scales to accurately capture mean ice draft and spatial variability.

Offshore from Wilkes Land

The floes surveyed in pack ice off Wilkes Land, East Antarctica, also revealed mostly thick (mean 2.72 m) ice with complex morphologies. Floe 8 had a rubble-field deformation pattern (Fig. 2c) and ice draft distribution (Supplementary Fig. 3) similar to that observed for Floe 1 in the Bellingshausen Sea. Extreme deformation was also observed on Floe 10, with the draft distribution of both floes showing long tails (Supplementary Fig. 3) and a significant fraction of ice thicker than 5 m. The latter floe also held ice with the greatest draft observed anywhere in the data set (16.2 m). The level ice draft for these floes (mean of 1.28 m) was thinner than for either the Weddell or Bellingshausen Sea, which is consistent with previous observations of sea-ice thickness[17] and the overall thinner ice for the Wilkes Land data, despite similar levels of deformation.

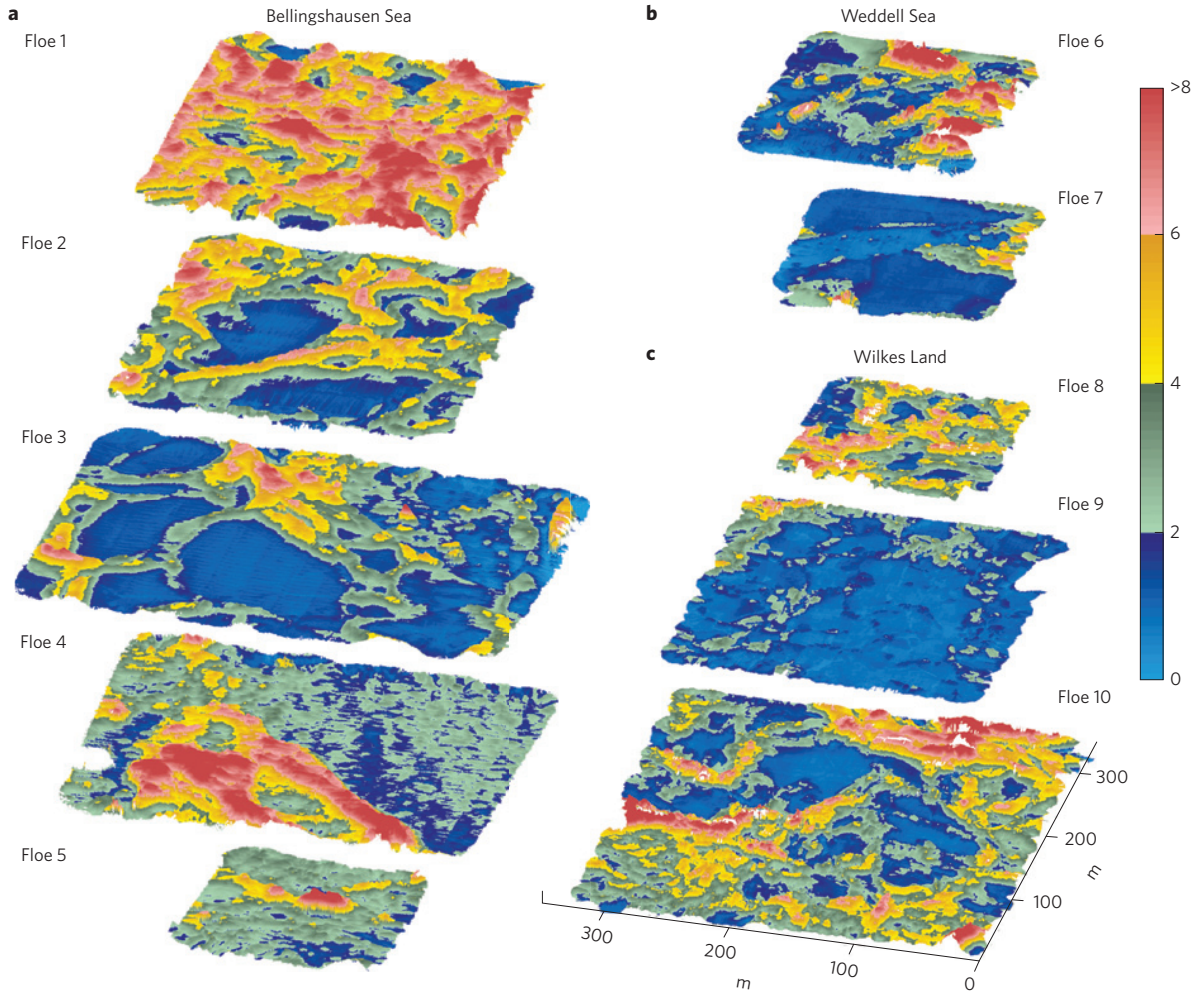

Figure 2 | 3D floe-scale sea-ice draft maps. a, Floes 1–5 from the Bellingshausen sector during IceBell (Fig. 1a). **b**, Floes 6–7 from the Weddell sector during IceBell (Fig. 1b). **c**, Floes 8–10 from Wilkes Land, East Antarctica during SIPEX-2. The colour scale is sea-ice draft (m). Horizontal scale is shown for Floe 10.

Comparison of AUV ice draft with previous observations

Previous observations of sea-ice thickness from visual shipboard observations and drilling data show a thin ice cover, but with modest seasonal and regional variability[12,17]. The probability distribution functions (PDFs) of the ice draft from the AUV data are compared against regional ASPeCt shipboard and drilling data (Fig. 3) from previous cruises that covered the most similar areas and season (see subpanels in Fig. 1). Only ASPeCt shipboard observations in September–November are included. The drilling data comes from selected voyages listed in Supplementary Table 2. These data do not provide a direct comparison to the AUV data, but demonstrate whether potential spatial and/or temporal sampling biases exist. ULS ice draft data, relatively unbiased by sampling issues, from two moorings in the western and central Weddell were also compared against the AUV data in the western Weddell (Fig. 3b).

In all regions, both the ASPeCt thickness and drilling draft data are well below (up to 70%) those shown in the AUV data. In part, this is because the ASPeCt data captures thin ice that is not sampled by drilling or AUV surveys (for these surveys, the AUV stayed under a single floe, and so did not transit under thin ice or brash between floes). The drilling data are expected to be more comparable. The modal drafts of the drilling data average about 50% thinner than those of the AUV data. This difference is significantly greater than observed seasonal variability[17]. The thicker level ice in the AUV data may reasonably be attributed to the combined differences in season and sampling location; the AUV data were acquired in areas less likely to be accessible to ships during spring.

ASPeCt observations show a similar distribution to drilling data, but also include some observations of thicker ice that is typically not drilled. The ASPeCt data are average thicknesses observed over 6-nautical-mile segments; as such, they cannot be compared directly with the full draft distributions provided by drilling or AUV data. Previous *in situ* data do not capture the very thick ice to the degree seen in the AUV data. For example, almost 80% of both the ASPeCt and drilling data have thickness/draft < 1 m, and almost 100% of the measurements have a thickness/draft < 3 m (see also Supplementary Fig. 4). In contrast, each of the AUV floe distributions has a long tail of thick ice (Fig. 3; distributions for each floe are shown in Supplementary Fig. 3). More than 90% of the ice draft is greater than 1 m, 40% of the ice draft is thicker than 3 m, and almost 20% thicker than 5 m. This is an approximate upper limit for drilling surveys, which would probably underestimate the mean draft of these floes by about 20%. This long tail in the distribution represents heavily deformed ice, as for Floe 7 and Floe 9, which both contain predominantly level ice with ice draft distributions most closely resembling the drilling data (Supplementary Fig. 3). The ULS data for the western and central Weddell Sea (Fig. 3b) show a large proportion of very thin ice, but also a peak that coincides with that of the AUV data, and a similar long tail, demonstrating that such under-ice measurements capture a portion of the draft distribution that is absent in the drilling data.

Table 1 | AUV floe survey statistics.

Floe	Area (10^4 m^2)	Level Ice Draft (m)	Mean Ice Draft (m)	Max Ice Draft (m)	Std Ice Draft	% area Def.	% vol. Def.
Bellingshausen sector							
1	5.3	1.85	5.48	11.55	1.79	91	97
2	5.4	1.35	3.18	8.36	1.54	69	85
3	8.0	1.20	2.25	9.15	1.40	48	72
4	6.9	2.00	3.44	17.58	2.02	40	62
5	2.0	1.55	2.98	10.26	1.16	72	82
(1–5)	27.5	1.59	3.46	11.55	1.57	64	80
ASPeCt		0.52	0.84	10.1	0.92	13	46
DRILL		0.91	1.16	5.01	0.74	33	41
Weddell sector							
6	3.4	1.50	3.10	13.82	2.31	41	69
7	3.3	1.20	1.70	8.16	1.06	28	50
(6–7)	6.7	1.50	2.40	13.82	1.68	34	59
ASPeCt		0.90	1.01	2.18	0.50	12	35
DRILL		1.00	1.05	2.88	0.40	9	15
ULS		-	2.21	-			
Wilkes Land sector							
8	2.5	1.50	3.60	11.47	1.60	76	90
9	6.8	0.80	1.42	8.24	0.84	45	66
10	11.1	1.55	3.30	16.20	1.87	65	84
(8–10)	20.1	1.28	2.77	16.20	1.44	62	80
ASPeCt		0.45	0.57	3.12	0.48	10	29
DRILL		0.65	0.90	5.26	0.53	15	27
Circum-Antarctic							
AUV	54.5	1.48	3.04	16.2	1.55	57	76
ASPeCt		0.53	0.82	10.1	0.77	12	43
DRILL		0.85	1.05	5.01	0.57	19	28

Level, mean, maximum and standard deviation of AUV ice draft (m) for each floe. ASPeCt ship-based thickness (m) and drill line ice draft (m), together with ULS draft (m), are included for comparison, as detailed in Figs 1 and 3. Deformed ice is defined as that greater than 1.5 times the level ice draft/thickness for computation of percentage area and volume of deformed ice.

Contribution of deformation to thickness distribution

The thickness distribution of Arctic ice generally follows a negative exponential for thicker ice[29,30]. While both the previous drilling data and AUV data exhibit an exponential drop-off for thicker ice, this occurs at a much thicker threshold for the AUV data ($\gtrsim$8 m) than for the drilling data ($\gtrsim$1 m). The draft distribution is relatively flat for ice between the level ice thickness (1–2 m) and the thickest ridges (8 m). Examination of PDFs for individual floes (Supplementary Fig. 3) shows that this is due to very high levels of deformation. This is predominantly rubble ice, which can form ice several metres thick without significant compression of the ice to form ridges.

The exponential drop-off of the Arctic ice thickness distribution has been attributed to the superposition of many ridges, with individual ridges tending to create a more level PDF (ref. 29). In the present data, the most deformed floes show a broad, largely flat PDF (that is, floes 1, 2, 5, 8 and 10 in Supplementary Fig. 3). We then see that the flat distribution is from a random jumble of ice that, rather than piled to form a classic pressure ridge, has frozen in place as a rubble field. The long tail of the PDF is composed of thicker, deformed ice structures. As seen in the draft maps, these are not generally long linear features, but isolated ridge fragments or rubble piles.

The lack of coherent ridge structures argues against classic ridge building typical of Arctic ice, where long, linear features composed of a large number of individual ice blocks form during individual shear or compression events. Large Arctic-type ridges are well known to not be the norm for Antarctic deformation features[21]. While the precise mechanisms driving deformation may vary among regions, the ice morphology suggests that a major driver of thickening may be the breakup of floes through repeated collisions or shear events and subsequent consolidation into rubble fields. We suggest that ice may mechanically thicken to mean thicknesses exceeding anything previously sampled by drilling without the need for the large ice stresses required for production of thick ridges.

For the ASPeCt data, ridged ice comprises 11% of the sea-ice area and increases the average ice thickness by about 35–40% in spring[17], based on the size and prevalence of observed ridge sails. For the subset of the data used for comparison in the present study, deformed ice contributes 43% to the ice volume (Table 1). In the comparable drilling data, the deformed ice area (defined as ice $>$ 1.5 times the level ice thickness—see Methods) is $\sim$19%, contributing $\sim$28% to the total ice mass. This is less than previous estimates of $\sim$40–50% (refs 21,31), as our criterion for deformed ice excludes most ice less than 1–1.5 m thick, which includes relatively thin deformation features that would have been included in previous analyses.

The percentage of deformed ice present in the surveys can be estimated by several criteria (Methods). For the AUV data, on average 57% of the area is deformed (Table 1), contributing an average of 76% to the total ice mass, which far exceeds that estimated from previous shipboard observations and drilling data. The contribution to the total volume is approximately two to three times that of the previous drilling and shipboard observations. Even for cruises that have inferred similar levels of deformation[31],

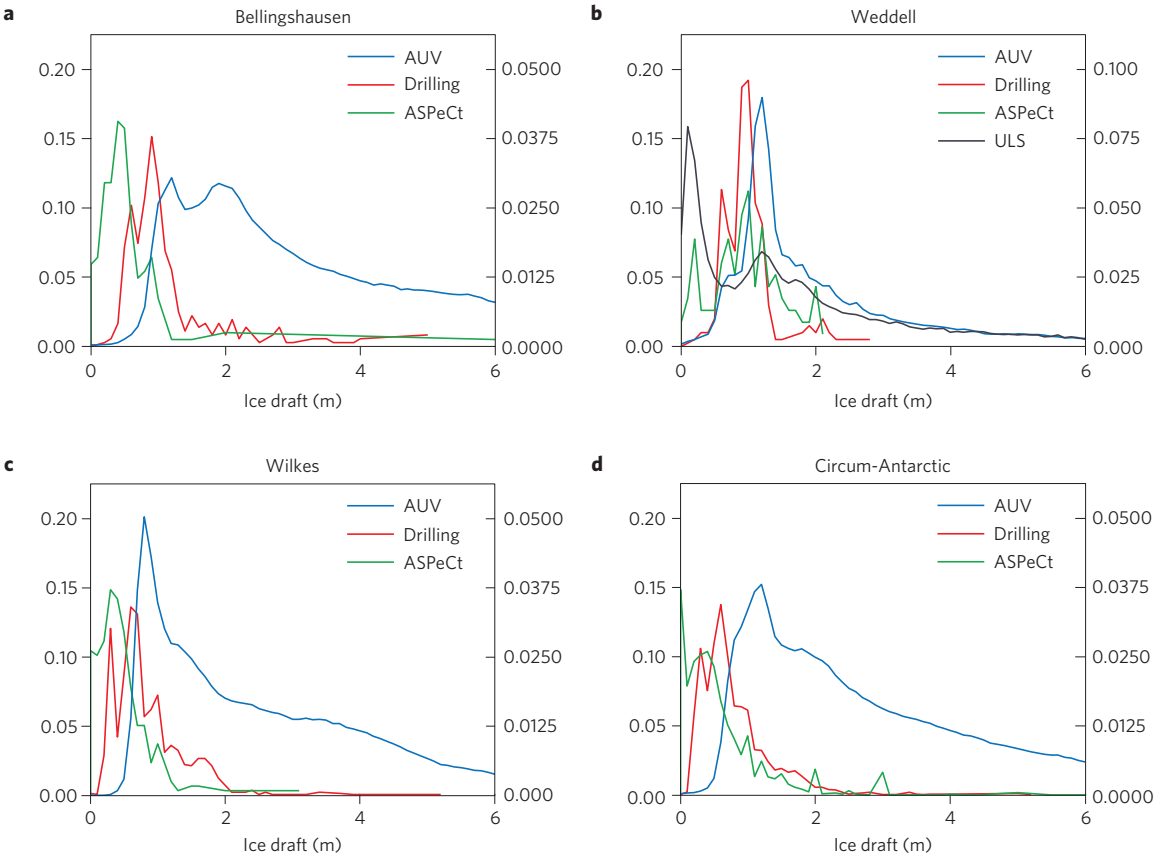

Figure 3 | Ice draft thickness distribution. Normalized histograms (probability distribution functions, or PDFs). Left *y*-axes for ice draft from ASPeCt drilling[12] (see Supplementary Table 2) and ASPeCt ship-based thickness estimates[17] (September–November), and right *y*-axes for ice draft from AUV and ULS (ref. 14, October data from sites 207 and 217 in the Weddell sector). **a**, Bellingshausen. **b**, Weddell Sea. **c**, SIPEX-2. **d**, All data. In **a**–**c**, data is included only within each region as shown in Fig. 1. Panel **d** includes all September–November data as shown in the inset of Fig. 1 and listed in Supplementary Table 2.

the mean draft in the present data is two to four times that reported in most other studies. In the few cases where ice of similar thickness has been reported, quantitative information on its morphology could not be measured[19], As such, the extent, scale, and detail of the deformation observed in the AUV data are exceptional.

Sampling bias in Antarctic sea-ice thickness estimates

The prevailing view of global sea ice is that the Antarctic pack is much thinner than the Arctic. The 3D maps of sea-ice draft presented here demonstrate deformation features significantly thicker than previously measured. This suggests that spatial/temporal sampling biases may exist in these previous data sets due to inability to access the thicker ice of the near-coastal regime, or avoidance of heavily deformed ice throughout the pack.

The question remains as to how representative the AUV draft measurements presented here are of the broader ice thickness distribution in near-coastal regions, and elsewhere, in spring. Ice with ridge sail heights exceeding 2–3 m or more have been inferred from airborne lidar measurements[32,33], The estimated contribution of these ridges to total ice volume is often >50%; however, they contribute only 0.5–1 m to the area-averaged ice thickness[32,33]—less than half the contribution of deformed ice to the average AUV draft. Since ridges are identified in lidar data by prominent surface features only, these data will underestimate the full extent of deformation captured by the AUV data.

Several recent remote sensing observations suggest that such thick ice may be more widespread. Freeboard data from NASA's Ice Cloud and land Elevation Satellite (ICESat) show broad bands of thick ice along the Bellingshausen/Amundsen coast[27] and the Western Weddell[25,28] that have been largely inaccessible to *in situ* sampling in spring from ships[24]. Observations of snow depth and total freeboard one month earlier in the same region of the Bellingshausen Sea suggest thick ice broadly consistent with the AUV measurements[34]. These high freeboards are not restricted to the limited regions sampled here, which suggests, along with the fact that thick, heavily deformed ice was observed consistently in all three regions, that such ice conditions may be more prevalent in the Antarctic spring sea-ice cover than has been previously observed. However, given the difficulties in comparing different sparse data sets from different areas and years, more direct comparisons are needed to determine how much the overall thickness of Antarctic sea ice may have been underestimated.

The floe-scale maps of sea-ice draft presented here provide a new perspective on Antarctic sea-ice thickness and deformation that has not previously been available. Demonstrating the ability of such AUV surveys to enhance our understanding of the role of deformation processes in controlling total sea-ice volume, these data provide evidence that thick ice in the near-coastal and interior pack may be under-represented in present *in situ* assessments of Antarctic sea ice. To determine whether such thick ice and deformation is more widespread throughout the Antarctic pack—with concomitant implications for our understanding of ice dynamics, production and ocean interactions—will require broader scale under-ice surveys, particularly in areas and in seasons that have been traditionally inaccessible to *in situ* measurements. Such assessments are needed before robust evaluation of sea-ice models and remotely sensed sea-ice thickness can be made.

Methods

Sea-ice draft is the component of thickness that is below sea level (total thickness combines draft and freeboard). Draft was used for all data (AUV, ULS, ASPeCt drilling) with the exception of the ASPeCt ship-based data (sourced from http://aspect.antarctica.gov.au/data). For ASPeCt ship-based observations, the difference is typically a few cm or less. For the AUV data, the difference may be as much as 25 cm, but does not impact comparisons made herein.

IceBell and SIPEX-2 cruises. The high-resolution geolocated 3D maps of sea-ice draft presented in Fig. 2 were collected during the United Kingdom-led Ice Mass Balance in the Bellingshausen Sea (IceBell) voyage to the Weddell and Bellingshausen seas in November 2010 (Floes 1–7) and the Australian-led Sea Ice Physics and Ecosystem Experiment II (SIPEX II) to East Antarctica in September–October 2012 (Floes 8–10). Floes 1–5 were surveyed on the continental shelf of the Bellingshausen Sea, with Floes 1–4 west of Alexander Island and Wilkins Sound, and Floe 5 at the southern end of Marguerite Bay at the ice front of George VI sound. Floes 6–7 were near-adjacent floes over the continental slope in the Weddell Sea, northeast of the Larsen Ice Shelf. Floes 8–10 were sampled over the continental rise offshore from the Sabrina Coast of Wilkes Land. We broadly classify these floes as part of the coastal pack ice regime (see Supplementary Table 3 for details of the location and dates of the floe surveys).

AUV survey methodology. Both expeditions used the Seabed-class autonomous underwater vehicle from the Woods Hole Oceanographic Institution (WHOI) equipped with a swath multibeam sonar. During IceBell and SIPEX II the ship was periodically moored at suitable ice floes across the sea-ice zone to conduct ice stations. The Seabed AUV was deployed and recovered from the stern of the ship through a relatively small pool of open water. A floe-referenced navigation frame is enabled through the use of long-baseline transponders deployed from the sea ice outside the survey area. The AUV uses an inertial navigation system using a true north-seeking Octans 3000 fibre optic gyro aided by an RDI Workhorse Doppler Velocity Log (DVL) measuring speed relative to the ice to provide navigation control. Operating at a depth of 20–30 m and driving in a lawnmower pattern with overlapping swaths, the AUV measures distance to the ice with a 245 kHz Imagenex deltaT37 multibeam sonar providing a horizontal resolution better than 0.25 m. The vertical error in draft is estimated to be less than 10 cm. Further details on the multibeam processing and estimation of errors are provided in the Supplementary Information.

Draft and deformation statistics. For computation of draft statistics and percentages of deformed ice for previous drilling data, the statistics were computed for each floe, and then the overall averages were weighted by the length of the profile. This was done because the level ice draft varied from floe to floe and the profiles often varied greatly in length. This reduced any bias by short profiles that were often more level than longer profiles. For the ship-based ASPeCt observations, the deformed ice volume was estimated from reported spring regional averages of areal extent of ridging, level ice thickness, and equivalent ice thickness[17].

The percentage of deformed ice present in the surveys can be estimated by several criteria. The traditional Rayleigh criteria used for identifying ridges in the Arctic[35] and for airborne lidar surveys of ridge sails in the Antarctic[32,33] is not appropriate for many Antarctic features, particularly rubble fields which may consist of many ridge-keel like features[21]. Here, we define deformed ice as ice thicker than 1.5 times the level ice draft. The level ice draft is defined as the modal ice draft, or the first significant peak of the ice draft distribution (in cases where the modal draft obviously includes deformed ice). This criterion is similar to the Rayleigh criteria used previously[32,35], but is more conservative, in that it will exclude regions of thinner ice found within rubble fields. We use a simple criterion, as it appears to capture most of the deformed ice areas, and a more sophisticated method that accounts for the local morphology[36] may not produce results directly comparable to those from the other data sets.

Received 31 March 2014; accepted 21 October 2014; published online 24 November 2014

References

1. Parkinson, C. L. & Cavalieri, D. J. Antarctic sea ice variability and trends, 1979–2010. *The Cryosphere* **6,** 871–880 (2012).
2. Sigmond, M. & Fyfe, J. C. The Antarctic sea ice response to the ozone hole in climate models. *J. Clim.* **27,** 1336–1342 (2014).
3. Bitz, C. M. & Polvani, L. M. Antarctic climate response to stratospheric ozone depletion in a fine resolution ocean climate model. *Geophys. Res. Lett.* **39,** L20705 (2013).
4. Bintanja, R., van Oldenborgh, G. J., Drijfhout, S. S., Wouters, B. & Katsman, C. A. Important role for ocean warming and increased ice-shelf melt in Antarctic sea-ice expansion. *Nature Geosci.* **6,** 376–379 (2013).
5. Holland, P. R. & Kwok, R. Wind-driven trends in Antarctic sea-ice drift. *Nature Geosci.* **5,** 872–875 (2012).
6. Massonnet, F. *et al.* A model reconstruction of the Antarctic sea ice thickness and volume changes over 1980–2008 using data assimilation. *Ocean Modelling* **64,** 67–75 (2013).
7. Zhang, J. Modeling the impact of wind intensification on Antarctic sea ice volume. *J. Clim.* **27,** 202–214 (2014).
8. Turner, J. *et al.* An initial assessment of Antarctic sea ice extent in the CMIP5 models. *J. Clim.* **26,** 1473–1484 (2013).
9. Comiso, J. C., Kwok, R., Martin, S. & Gordon, A. L. Variability and trends in sea ice extent and ice production in the Ross Sea. *J. Geophys. Res* **116,** C04021 (2011).
10. Martinson, D. G. & Iannuzzi, R. A. in *Antarctic Sea Ice: Physical Processes, Interactions and Variability* (ed. Jeffries, M.) 243–271 (AGU, 1998).
11. Kwok, R. & Rothrock, D. A. Decline in Arctic sea ice thickness from submarine and ICESat records: 1958–2008. *Geophys. Res. Lett* **36,** L15501 (2009).
12. Ozsoy-Cicek, B., Ackley, S., Xie, H., Yi, D. & Zwally, J. Sea ice thickness retrieval algorithms based on *in-situ* surface elevation and thickness values for application to altimetry. *J. Geophys. Res.* **118,** 3807–3822 (2013).
13. Harms, S., Fahrbach, E. & Strass, V. H. Sea ice transports in the Weddell Sea. *J. Geophys. Res.* **106,** 9057–9073 (2001).
14. Behrendt, A., Dierking, W., Fahrbach, E. & Witte, H. Sea ice draft in the Weddell Sea, measured by upward looking sonars. *Earth Syst. Sci. Data* **5,** 209–226 (2013).
15. Haas, C. Evaluation of ship-based electromagnetic-inductive thickness measurements of summer sea-ice in the Bellingshausen and Amundsen Seas, Antarctica. *Cold Reg. Sci. Technol.* **27,** 1–16 (1998).
16. Weissling, B., Lewis, C. L. & Ackley, S. F. Sea ice thickness and mass at Ice Station Belgica, Bellingshausen Sea, Antarctica. *Deep-Sea Res. II* **58,** 1112–1124 (2011).
17. Worby, A. P. *et al.* Thickness distribution of Antarctic sea ice. *J. Geophys. Res.* **113,** C05S92 (2008).
18. Jeffries, M. O. *et al.* Crystal structure, stable isotopes (δ^{18}O), and development of sea ice in the Ross, Amundsen, and Bellingshausen seas, Antarctica. *J. Geophys. Res.* **99,** 985–995 (1994).
19. Massom, R. A. *et al.* Extreme anomalous atmospheric circulation in the West Antarctic Peninsula region in Austral Spring and Summer 2001/02, and its profound impact on sea ice and biota. *J. Clim.* **19,** 3544–3571 (2006).
20. Adolphs, U. Ice thickness variability, isostatic balance and potential for snow ice formation on ice floes in the south polar Pacific Ocean. *J. Geophys. Res.* **103,** 24675–24691 (1998).
21. Tin, T. & Jeffries, M. O. Morphology of deformed first-year sea ice features in the Southern Ocean. *Cold Reg. Sci. Technol.* **36,** 141–163 (2003).
22. Timmermann, R., Worby, A., Goosse, H. & Fichefet, T. Utilizing the ASPeCt sea ice thickness data set to evaluate a global coupled sea ice-ocean model. *J. Geophys. Res.* **109,** C07017 (2004).
23. Holland, P. R. *et al.* Modelled trends in Antarctic sea ice thickness and volume. *J. Clim.* **27,** 3784–3801 (2014).
24. Jeffries, M. O. *et al.* in *Antarctic Sea Ice: Physical Processes, Interactions and Variability* (ed. Jeffries, M.) 89–122 (AGU, 1998).
25. Yi, D., Zwally, H. J. & Robbins, J. ICESat observations of seasonal and interannual variation of sea-ice freeboard and estimated thickness in the Weddell Sea, Antarctica. *Annu. Glaciol.* **52,** 43–51 (2011).
26. Worby, A. P. *et al.* Regional-scale sea-ice and snow thickness distributions from *in situ* and satellite measurements over East Antarctica during SIPEX 2007. *Deep Sea Res. II* **58,** 1125–1136 (2011).
27. Xie, H. *et al.* Sea ice thickness estimations from ICESat Altimetry over the Bellingshausen and Amundsen Seas, 2003–2009. *J. Geophys. Res.* **118,** 2438–2453 (2013).
28. Kurtz, N. T. & Markus, T. Satellite observations of Antarctic sea ice thickness and volume. *J. Geophys. Res.* **117,** C08025 (2012).
29. Wadhams, P., Wilkinson, J. P. & McPhail, S. D. A new view of the underside of Arctic sea ice. *Geophys. Res. Lett.* **33,** L04501 (2006).
30. Wadhams, P. & Davy, T. On the spacing and draft distributions for pressure ridge keels. *J. Geophys. Res.* **91,** 10697–10708 (1986).
31. Worby, A. P. The thickness distribution of sea ice and snow cover during late winter in the Bellingshausen and Amundsen seas, Antarctica. *J. Geophys. Res.* **101,** 28441–28455 (1996).
32. Weeks, W. F., Ackley, S. F. & Govoni, J. Sea ice ridging in the Ross Sea, Antarctica, as compared with sites in the Arctic. *J. Geophys. Res.* **94,** 4984–4988 (1989).
33. Dierking, W. Laser profiling of the ice surface topography during the Winter Weddell Gyre Study 1992. *J. Geophys. Res.* **100,** 4807–4820 (1995).
34. Kwok, R. & Maksym, T. Snow depth of the Weddell and Bellingshausen sea ice covers from IceBridge surveys in 2010 and 2011: An examination. *J. Geophys. Res.* **119,** 4144–4167 (2014).

35. Lowry, R. & Wadhams, T. P. On the statistical distribution of pressure ridges in sea ice. *J. Geophys. Res.* **84,** 2487–2494 (1979).
36. Wadhams, P. & Horne, T. P. An analysis of ice profiles obtained by submarine sonar in the Beaufort Sea. *J. Glaciol.* **25,** 401–424 (1980).

Acknowledgements

We are grateful for the professionalism of the officers, crew and technical staff of the RSS J. C. Ross (IceBell) and RV Aurora Australis (SIPEX-II). J. Pietro from the Woods Hole Oceanographic Institution and R. Frost and P. Alexander from the Australian Maritime College at the University of Tasmania provided assistance in the field. K. Meiners, A. Steer, P. Heil and R. Massom (AAD), and R. Scharein (UVic) provided ice and snow properties data. C. Dietz (UTAS-CSL), A. Moy (AAD) and E. Rohling (NOC) analysed the oxygen isotope data. This work was supported by the Australian Government's Cooperative Research Centres Programme through the Antarctic Climate and Ecosystem Cooperative Research Centre. Support for the IceBell cruise was supplied by the British Antarctic Survey and NERC grant NE/H009620/1. Support for the SIPEX-2 cruise was through the Australian Antarctic Science Grant No. 4073. T.M. was supported in part by NSF grant OPP-1142075. H.S. was supported by NSF grant ANT-1039951.

Author contributions

J.W., T.M. and G.W. conceived and led the fieldwork. H.S., C.K., C.M. and P.K. developed the AUV and operated it in the field. C.K. processed the multibeam and AUV data. G.W., T.M. and J.W. wrote the paper.

Additional information

Supplementary information is available in the online version of the paper. Reprints and permissions information is available online at www.nature.com/reprints.
Correspondence and requests for materials should be addressed to G.W., T.M. or J.W.

Competing financial interests

The authors declare no competing financial interests.